16th World Conference on Earthquake, 16WCEE 2017
Santiago Chile, January 9th to 13th 2017
Paper N° 4144 (Abstract ID)
Registration Code: S-H1462529088

GROUND MOTION PREDICTION EQUATIONS FOR MINING INDUCED SEISMICITY IN LEGNICA GLOGOW COPPER DISTRICT IN POLAND

S. Lasocki[1], D. Olszewska[2]

[1] Professor, Institute of Geophysics, Polish Academy of Sciences, lasocki@igf.edu.pl
[2] PhD, Institute of Geophysics, Polish Academy of Sciences, dolszewska@igf.edu.pl

Abstract

Compared to tectonic earthquakes, the seismic events induced by technological activity are weak to moderate but due to their shallowness they can result in significant ground motion. Furthermore, specific features of such seismic sources cause that the ground effects of these events do not follow ground motion propagation rules worked out from observations of tectonic earthquakes. In particular, these ground effects depend on source directivity and path and site properties much stronger than the ground motion due to tectonic earthquakes. Following, the ground motion prediction equation should be site-specific and should take into account source mechanism and space-time clustering of sources.
We present here new ground motion prediction equations, relevant for mining seismic activity in underground copper mines in Legnica-Glogow Copper District in Poland which have been developed taking into account the above considerations. The ground motion database, comprising 4533 signals, makes it possible to split ground motion prediction equations into classes, linked to similar source mechanisms or linked to similar locations. It has turned out that the normal and odd faulting events induce in general stronger motion than the thrust faulting and non-DC events. Also the membership of seismic sources to particular clusters of seismicity has proved to discriminate significantly the resultant ground motion amplitudes. This effect seems to be related to mining conditions.

Keywords: ground motion prediction, mining seismicity, site effect

1 Introduction

Anthropogenic earthquakes, that is those induced by underground mining, conventional and unconventional extraction of hydrocarbons, hydro- and geothermal energy production etc., result in ground motion, which can have a damaging impact on surface structures. Reliable prediction of such ground motion is essential for protecting surface objects against the destructive effects of seismic events.

Ground motion prediction equations (GMPE), relate ground motion amplitude parameters, to sets of independent variables representing the cause of the motion. The surface impact of a seismic event at a site depends primarily on the event size and the source-to-site distance. Therefore, the primary independent variables included in the ground motion prediction models are seismic event magnitude and source-receiver distance [8]. Local conditions at the site are also crucial for the size of the seismic effect [13]. Their influence appears as a local amplification of ground motion. The relation between an amplitude parameter and the independent variables representing the mentioned factors most often takes a form of regression [e.g. 1, 2, 3, 4, 6 and 15, 16, 17, 18, 19 20 for areas of mining induced seismicity].

GMPE-s are developed based on ground motion data recorded during earthquakes. The conditions of ground vibration propagation and the amplifying effects at site are related to geological conditions of the area of interest. Therefore, in order to obtain an accurate tool for predicting the ground motion, the identification of GMPE should be done locally, to account for these local conditions. This is especially valid for effects of anthropogenic earthquakes, where the sources are weak and shallow, hence the extent of their impacts is conditioned strongly by local geology.

In this paper we analyse ground motion caused by the seismicity induced by mining activity in the Legnica Glogow Copper District (LGCD) in Poland. Underground copper-ore mining in LGCD, carried on in three mines at the depth from 900 to 1200 m, is accompanied by intense induced seismicity. Yearly about

2.5 thousand events of local magnitude above 1.0 are registered. Occasionally, events of magnitude M4 and stronger occur. This seismic activity gives rise to considerable ground motion, which affects buildings and other surface structures from the area.

To control the level of seismic hazard for the surface objects, ground motion has been monitored for dozens of years with a dense network of accelerometric stations. The already gathered abundant ground motion database makes it possible to identify GMPE variants, which, in addition to source size and source-receiver distance, take into account also other factors determining ground motion amplitude.

It has been evidenced that the type of faulting mechanism should be taken into considerations when estimating ground motion. GMPE models for tectonic seismicity, including dependence on magnitude, source-receiver distance, site effect and style of fault has been presented e.g. in [4, 8].

In this paper we identify GMPE-s for peak values of ground motion acceleration for the LGCD region, which include relative site effects. By splitting the ground motion database into groups linked to similar source mechanism as well as linked to similar locations, we investigate changes of GMPE-s in relation to source mechanism type and time-space location of sources.

2 Data

The analyzed ground motion database comprise records from 22 ground motion stations from the period from 2004 to 2013. The station ID numbers and locations are provided in Table 1 and also shown in Figure 2. The closest distance between the stations is 89 m and the farthest distance is 9322 m. The network covers an area of about 69 km^2. These records have been accepted for further analysis, whose peak horizontal acceleration (PHA) was greater than 0.03 m/s^2 and magnitude of the source was no less than 2.0. The selected database has consisted of altogether 4533 records. Source-receiver epicentre distances range from 31 m to 8634 m with a median value 1581 m.

Table 1 – Locations of accelerometric stations. The coordinates are in Polish 2000 coordinate system.

Station Ordinal Number	Station ID Number	X coordinate [m]	Y coordinate [m]
1	21	5707965	5574751
2	22	5705205	5576367
3	23	5708265	5573378
4	24	5708285	5574628
5	25	5712545	5575201
6	26	5705930	5579069
7	27	5707950	5575589
8	28	5712765	5579667
9	29	5711184	5576599
10	30	5710090	5577152
11	32	5710160	5577259
12	42	5709620	5580770
13	50	5712811	5581318
14	51	5710871	5579539
15	55	5711356	5582173
16	57	5710441	5581668
17	80	5707919	5574388
18	81	5708289	5574818
19	82	5709719	5580918
20	83	5708859	5574548
21	84	5708199	5573438
22	20	5708549	5574411

The selected accelerometric signals were triggered by 1605 seismic events from three seismically active mines. Figure 1 presents the distribution of the number of records from different sites, corresponding to the same event. More than 50% of seismic events triggered vibrations recorded only by one station. Only 28% of events led to signals recorded by four or more stations.

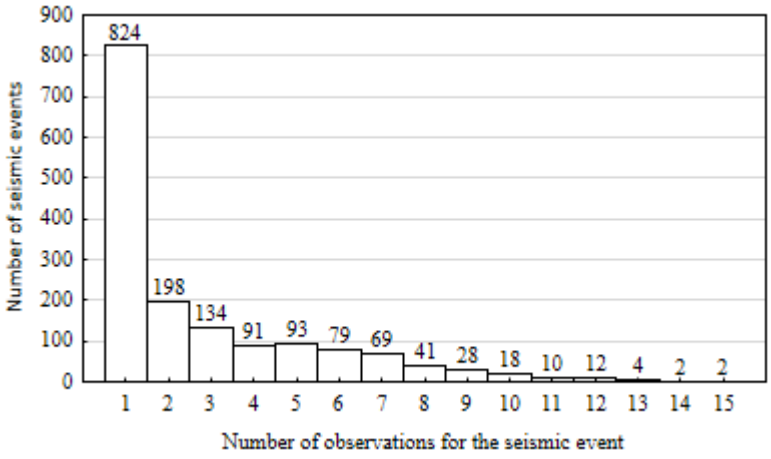

Fig. 1 – Distribution of the number of records from different stations, corresponding to the same event.

Seismicity induced by mining forms distinct space-time clusters or space-time zones [21]. The analyzed 1605 events formed 41 seismic zones. For the analysis of on the dependence of ground motion on the zones, to which sources belong, we have selected the most active nine zones and divided the set of accelerometric records into classes corresponding to the distinguished seismic zones. These are:

- R2 with 105 events (median M_L2.6, max M_L4.1) that induced 270 accelerometric records with max PHA=2.77 m/s^2,
- R3 with 106 events (median M_L2.7, max M_L3.6) that induced 424 records with max PHA=1.79 m/s^2,
- R6 with 94 events (median M_L2.5, max M_L3.8) that induced 229 records with max PHA=2.89 m/s^2,
- R12 with 127 events (median M_L2.3, max M_L3.4) that induced 452 records with max PHA=1.06 m/s^2,
- R13 with 107 events (median M_L2.4, max M_L3.5) that induced 486 records with max PHA=1.08 m/s^2,
- R17 with 52 events (median M_L2.5, max M_L4.0) that induced 236 records with max PHA=0.81 m/s^2,
- R22 with 87 events (median M_L2.6, max M_L3.7) that induced 239 records with max PHA=1.32 m/s^2,
- R25 with 149 events (median M_L2.6, max M_L3.6) that induced 498 records with max PHA=0.96 m/s^2,
- R26 with 170 events (median M_L2.3, max M_L3.7) that induced 247 records with max PHA=1.47 m/s^2.

The considered zones contain altogether 997 seismic events. These events resulted in altogether 3081 accelerometric records. The area distribution of the events from the zones are shown in Figure 2. Some of the zones overlap spatially, however then they are separated in time.

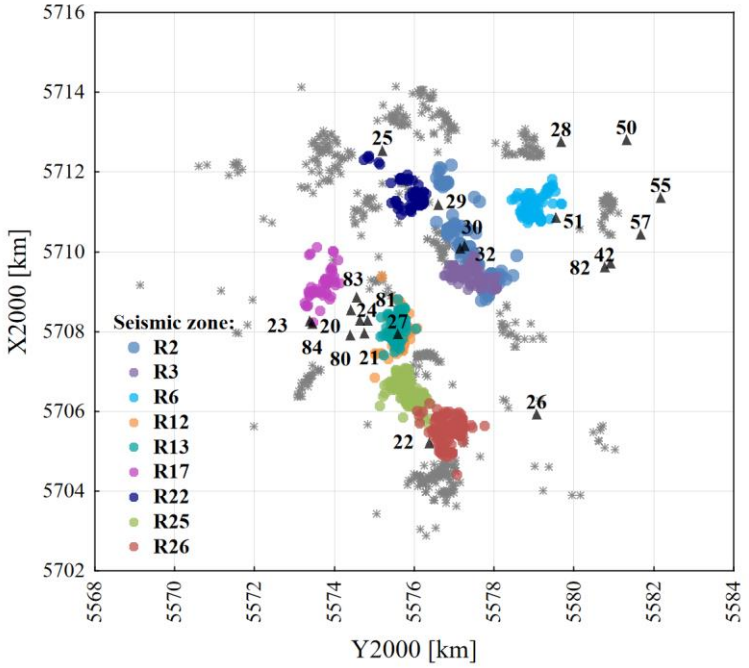

Fig. 2 – Location of ground motion monitoring stations and epicenters of seismic events, which induced accelerometric signals stored in the ground motion database. Triangles indicate locations of the monitoring stations and the numbers are stations' ID-s. Colored circles – epicenters of events from the nine zones selected to study; colors mark zone memberships. Gray stars – epicenters of events from other zones.

Next we have divided the set of accelerometric records with respect to the source mechanisms of the corresponding events. Out of the initial 1605, full moment tensor mechanism solutions were earlier evaluated for 298 sources. The solutions are available in an internal catalogue of mining induced seismic events from LGCD of the Institute of Geophysics, Polish Academy of Sciences. Focal mechanisms were calculated using the moment tensor inversion in time domain. The calculations were performed with the use of FOCI software [14], adjusted to the geological situation within the mine. The input parameters were the first amplitudes and polarities of P waves taken from in-mine seismic systems.

These 298 events have been classified according to type of focal mechanism. The events with dominating double couple component have been marked as DC and further on divided into groups of the same style of faulting according to the Frohlich and Apperson division [9]. The DC events has passed to the following faulting categories:

- the normal faulting class (N) comprises 41 events with median M_L2.6, which caused 129 ground motion records with maximum PHA equal 2.70 m/s^2,
- the thrust faulting class (T) comprises 90 events with median M_L2.8, which caused 395 records with maximum PHA equal 2.89 m/s^2,
- the odd faulting class (O) comprises 34 events with median M_L2.5, which caused 120 records with maximum PHA equal 0.96 m/s^2.

There are no Frohlich and Apperson's [9] strike-slip faulting events in the analysed group of DC sources.

The remaining 133 events have distinctly non-DC mechanisms. Such mechanisms are not unexpected in mining seismicity [10, 11]. These events have been divided as follows. The events with dominating compensated linear vector dipole (CLVD) component form a CLVD class. These are 77 events with median M_L2.8, which caused 270 records with maximum PHA equal 2.48 m/s^2. The events with all three components: isotropic, CLVD and DC having similar share of about 30% form a MIX class. These are 48 events with median M_L2.8, which caused 204 records with maximum PHA equal 1.68 m/s^2. For 8 events which remains, the isotropic component was the smallest and the share DC and CLVD components was similar. Because only 44 ground motion records are linked to these events these group is not considered when analysing the dependence of

GMPE on the mechanism type. Thus, the data selection with respect to the source mechanism resulted in a set of altogether 290 seismic events and 1118 accelerometric records.

In order to retain only the frequency components, which are important from an engineering point of view, the signals have been filtered with the 10 Hz low pas filter, and PHA values have been recalculated. There are four signals of the filtered PHA greater than 2 m/s^2. The strongest motion, with PHA=2.89 m/s^2, was measured by the station ID51. This motion was caused by the thrust faulting M_L3.3 event occurred on 20th September 2013. The event was located within R6 seismic zone, 610 m horizontally from the station. The second signal of PHA > 2 m/s^2, precisely PHA=2.77 m/s^2, was recorded by the station ID30 and was caused by the thrust faulting M_L3.6 event occurred on 19 July 2005, which was located within R2 zone some 500 m horizontally from the station. The third, PHA 2.7 m/s^2 at the station ID51, was caused by the normal faulting M_L3.2 event on 11 March 2012, located at the horizontal distance about 890 m within R6 seismic zone. The fourth case of PHA greater than 2 m/s^2, exactly 2.48 m/s^2 also recorded by ID51, was caused by the M_L3.2 event from zone R6, locates at the horizontal distance about 860 m.

3 Ground motion prediction equation

Following [16], where options of the epicentral distance inclusion are analysed and relative local amplification factors are considered in mining seismicity problems, the GMPE model to be identified here reads

$$\log PHA_k(M_L, r) = \alpha + \beta M_L + \gamma \log\sqrt{r^2 + h^2} + \sum_{n=1}^{N-1} \delta_k S_{kn}\,,\ k=1,\ldots,N \qquad (1)$$

where k is the station ordinal number, N is the number of stations, PHA_k is PHA at k-th station location, M_L is the event magnitude, r is the source-station epicentral distance, and h is the common depth factor introduced to account for the non-linearity of ground vibration propagation on short distances from the epicentre. h is estimated so that the standard error of estimation is the least [12]. The last term on the right hand side of Eq.1, $\sum_{n=1}^{N-1} \delta_k S_{kn}$, is introduced in order to account for relative local site effects. Here the station No. N is considered as a reference station and δ_k are the amplification coefficients. They are the logarithmized values of amplification at the site of the station No. k, with respect to the site of the station No. N. Obviously δ_N=0. S_{kn} is the Kronecker delta. The coefficients $\alpha, \beta, \gamma, \delta_k$ are estimated by means of the analysis of regression [7]. The free parameter of regression takes an individual value for each station location. Having estimated the station related free parameters one can work out a map of the relative amplification [16]. It should be noted that δ_k are the relative local site effects and not just the effects of amplification due to structure of overburden. They represent relative differences of ground motions at stations due to all factors other than those from the independent variables, i.e. the geometry and directivity of the sources, the properties of the paths and the site amplification.

The GMPE model from Eq. 1 is specific for stations (sites). As shown in Figure 1, there are few record from different stations corresponding to the same event. Therefore we do not account for correlations within each event. Otherwise we would have to exclude from the analysis more than 70% of records, which would make it impossible the whole study.

In order to estimate $\alpha, \beta, \gamma, \delta_k$ and h simultaneously, the linear regression analysis is repeated 5000 times for h changing from 1 to 5000 m and this set of coefficients $\alpha, \beta, \gamma, \delta_k$ is accepted, which result in the least standard error of estimate of the regression. Next, outliers are identified and removed from the data and the procedure is repeated. The analysis is continued until there are no distinct outliers.

4 Results of the analysis

4.1 General GMPE

The final GMPE, elaborated from the whole dataset takes the form of

$$\log PHA_k = -0.314 + 0.841 M_L - 0.977 \log\sqrt{r^2 + 409^2} + \delta_k \qquad (2)$$

The reference station is the station ID20. The amplification coefficients and relative amplification factors are provided in Table 2. The estimation has been based on 4000 ground motion records, whereas the remaining 533 have been discarded as generating outlying residuals. The coefficient of determination is 0.75 and the standard error of estimates is 0.161. Eq. 2 is further on referred to as the general GMPE.

The variability of site effects, expressed in terms of the relative amplification, is significant. For the same value of M_L and r, median PHA is 3.16 times bigger at station ID42 than at station ID83. The distance between these two stations is 6.24 km. The relative amplification at station ID22 with respect to the station ID21 is 1.35 where the distance between these two stations is only 3.2 km. (see: Table 2).

Table 2 – Relative amplification factors for PHA

Station Ordinal Number	1	2	3	4	5	6	7	8	9	10	11
Station ID Number	21	22	23	24	25	26	27	28	29	30	32
Amplification coefficient, δ_k	-0.13	0.04	0.09	-0.03	0.00	0.08	0.00	-0.06	0.02	0.03	0.11
Relative amplification	0.74	1.09	1.24	0.92	1.01	1.19	1.00	0.87	1.05	1.06	1.28
Station Ordinal Number	12	13	14	15	16	17	18	19	20	21	22
Station ID Number	42	50	51	55	57	80	81	82	83	84	20
Amplification coefficient, δ_k	0.34	0.08	0.09	0.10	0.16	0.01	-0.04	-0.05	-0.16	-0.02	0.0
Relative amplification	2.18	1.21	1.24	1.26	1.45	1.02	0.91	0.90	0.70	0.94	1.0

4.2 Dependence on source mechanism

To analyse the dependence of surface seismic effects on source mechanism of underground mine seismicity the data set related to 298 events with known mechanisms is used. Figure 3 shows means and confidence intervals of regression residuals of the general GMPE respectively in the mechanism categories. The negative mean residual in the thrust faulting category suggests certain overestimation of PHA by the general GMPE. To the contrary the mean residuals in all other mechanism categories are positive, which suggests underestimation of PHA be the general GMPE. However, only the odd faulting, normal faulting and to some extent MIX categories exhibit statistically significant deviations, whereas effects of thrust and CLVD mechanism events seem to be well constrained be the general GMPE. Thus it can be concluded that N, O and MIX events generate stronger motion than average for all types of sources together. This is different than in the case of natural tectonic events where stronger motion is due to thrust faulting earthquakes [4, 5, 8].

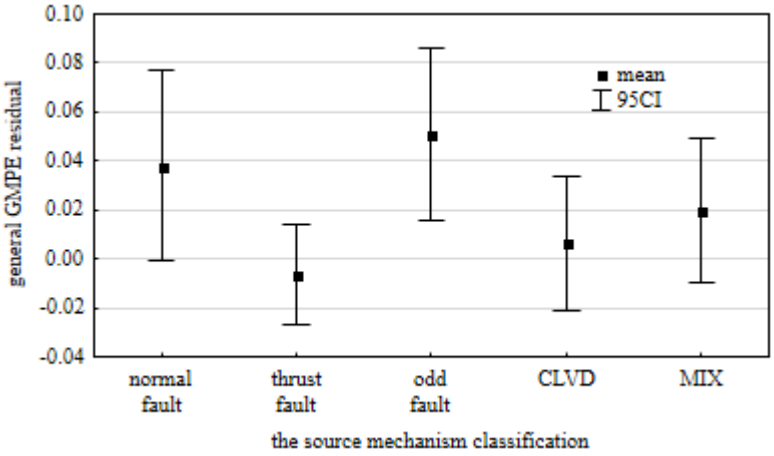

Fig. 3 – Regression residuals of the general GMPE against source mechanism classes.

The source mechanism-specific GMPE-s are presented by Eqs. (3-7) and the amplification coefficients are provided in Table A in the Appendix.

$$\log PHA_N = -0.707 + 1.210M_L - 1.164\log\sqrt{r^2 + 382^2} + \delta_k \quad (3)$$

$$\log PHA_T = -0.267 + 0.959M_L - 1.113\log\sqrt{r^2 + 401^2} + \delta_k \quad (4)$$

$$\log PHA_O = 0.888 + 0.918M_L - 1.403\log\sqrt{r^2 + 910^2} + \delta_k \quad (5)$$

$$\log PHA_{CLVD} = -0.141 + 0.871M_L - 1.060\log\sqrt{r^2 + 661^2} + \delta_k \quad (6)$$

$$\log PHA_{MIX} = -0.590 + 1.010M_L - 1.024\log\sqrt{r^2 + 527^2} + \delta_k \quad (7)$$

Figure 4 shows PHA estimations obtained using Eq. (2-7) as a function of local magnitude and distance for the reference station (ID20), for which the amplification coefficient δ=0.0. The dependence on magnitude at a fixed distance is shown in Figure 4 (left side). The distance is fixed to 1581 m, which is the median value of the source-receiver distance taken from all data. The dependence on the epicentral distance for a fixed magnitude is presented in Figure 4 (right side). The magnitude value is 2.8, which is the median value from all sources.

All mechanism-specific GMPE-s reveal stronger influence of magnitude on the ground motion amplitude than this influence is in the general GMPE. The relations between the dependence on magnitude for the particular mechanism types, shown in Figure 4, are same as they can be deduced from Eqs. 3-7.

Due to the presence in GMPE-s of the depth factor, *h*, which takes different values in particular equations, relations between the dependence on the epicentral distance for the mechanism types are more complex. Broadly, normal faulting results in the strongest horizontal ground motion at short epicentral distances. Yet, PHA due to this mechanism type decreases the fastest with the distance. The second strong impacts for short epicentral distances result from thrust faulting and MIX mechanisms and are similar to that predicted from the general GMPE. Odd faulting and CLVD mechanisms generate the lowest ground motion in the epicentral area. At the same time, the decrease of this ground motion with the distance is the slowest. At the distances of more than 1.5 km the differences between the impacts due to the particular mechanism types die down. Because the most important cases from an engineering point of view are effects of strong events at short epicentral distances it can be concluded that for such cases the differences between the effects linked to mechanism categories are significant. Hence the use of mechanism-specific GMPE-s, Eqs. 3-7, are recommended over the use of the general GMPE.

Interestingly, as shown in Table A in the Appendix, the site coefficients δ_k for the same receiving points differ for different mechanism types of as well as they differ from these coefficients in the general GMPE. This results from the above mentioned fact that these coefficients are related not only to the soil properties at sites, but also linked to source and path characteristics. In the studied case the differences in sources' directionality of

different mechanism types seem to be significant. These differences are exemplified in Figure 5 for DC sources. The strike angles of O events are mostly smaller than the strike angles of T and N events. Furthermore, they cluster at about 30°, at about 60° and at about 100-120°, whereas with some exception of 60° and N-class events, the events from the other two classes do not. The differences in dips are very distinct. The dip angles of T-class events are distinctly smaller, then those of the other two classes. The dip angles of O-class events are mostly the biggest, and the dips of N-class events cluster. Thus, the differences in δ_k-s may have come from these differences in sources' directionality. However, the detailed analysis of this topic is out of scope of the present paper.

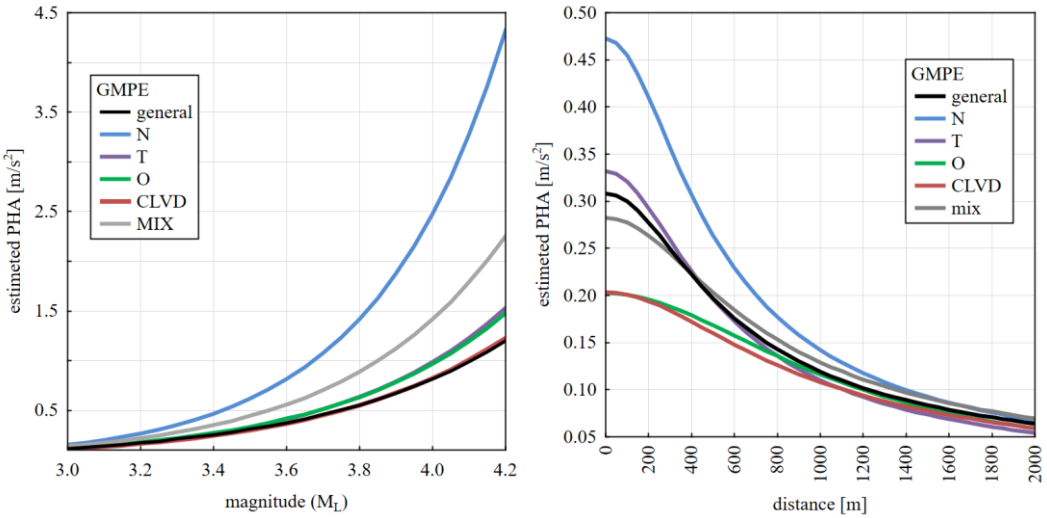

Fig. 4 – Comparison of PHA obtained from mechanism-specific GMPE-s. Left: PHA vs. magnitude at fixed epicentral distance. Right: PHA vs. epicentral distance at fixed magnitude.

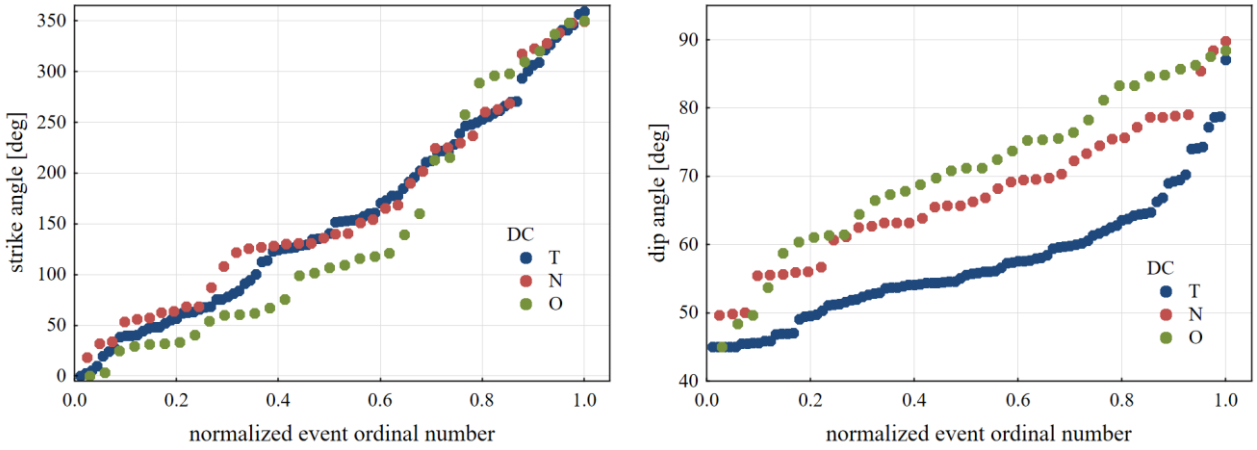

Fig. 5 – Orientations of fault planes of events from different classes of DC focal mechanism. Left: strike angles; Right: dip angles.

4.3 Dependence on seismic zone

The next considered subject is an influence of events provenience on ground motion. Figure 6 shows means and confidence intervals of regression residuals of the general GMPE, respectively for sources from the nine seismic zones. The differences between the mean residuals are significant. Effects of seismic events from zones R3, R6,

R25 are statistically significantly stronger, and effects of events from R2 and R17 are significantly weaker than those expected based on the general GMPE.

There are no conclusive regularities regarding the locations of the mentioned zones. To the contrary, the zones R3 - underestimated effects and the zone R2 - overestimated effects are more or less in the same place. The only common factor distinguishing the group: R3, R6, R25 from the group: R2, R17 is their period of activity. The seismicity of the first group zones began in 2003 (R6, R25) and 2006 (R3), and the zones R2 and R17 became active earlier, in 1990 and 2000, respectively. The time of zone activity is linked to the time of mining of that rockmass part where the zone is located. Thus, it seems that the mining time and the resultant actual mining situation may be responsible for the observed differences. However, the way in which the mining situation can influence propagation of vibrations remains unknown and the problem requires further detailed studies. Nevertheless, the significance of the differences from Figure 6 implicates the need to construct zone-specific GMPE-s.

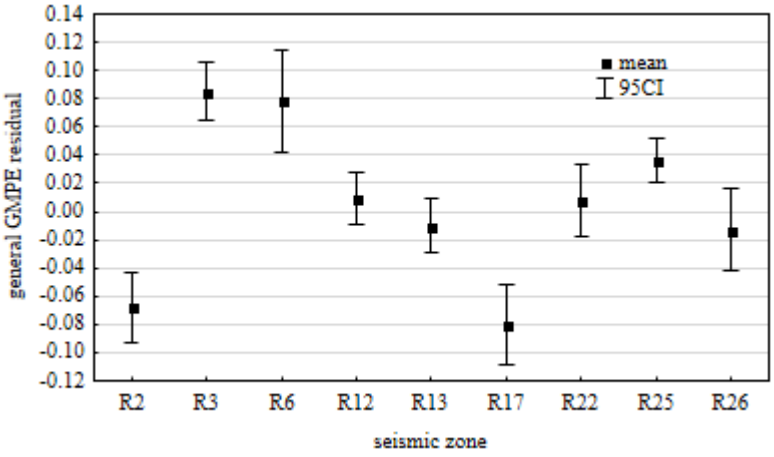

Fig. 6 – Regression residuals of the general GMPE against source mechanism classes.

The worked out zone-specific GMPE-s are:

$$\log PHA_{\mathrm{R2}} = -1.029 + 0.774 M_L - 0.728 \log\sqrt{r^2 + 94^2} + \delta_k \quad (8)$$

$$\log PHA_{\mathrm{R3}} = 3.739 + 0.923 M_L - 2.154 \log\sqrt{r^2 + 2281^2} + \delta_k \quad (9)$$

$$\log PHA_{\mathrm{R6}} = -4.940 + 1.316 M_L - 0.131 \log r + \delta_k \quad (10)$$

$$\log PHA_{\mathrm{R12}} = -2.992 + 1.105 M_L - 0.346 \log\sqrt{r^2 + 96^2} + \delta_k \quad (11)$$

$$\log PHA_{\mathrm{R13}} = 9.564 + 0.874 M_L - 3.969 \log\sqrt{r^2 + 1495^2} + \delta_k \quad (12)$$

$$\log PHA_{\mathrm{R17}} = 0.192 + 0.881 M_L - 1.198 \log\sqrt{r^2 + 592^2} + \delta_k \quad (13)$$

$$\log PHA_{\mathrm{R22}} = 3.337 + 1.074 M_L - 2.122 \log\sqrt{r^2 + 1506^2} + \delta_k \quad (14)$$

$$\log PHA_{\mathrm{R25}} = 10.568 + 0.780 M_L - 3.890 \log\sqrt{r^2 + 3254^2} + \delta_k \quad (15)$$

$$\log PHA_{\mathrm{R26}} = -1.874 + 0.796 M_L - 0.512 \log\sqrt{r^2 + 190^2} + \delta_k \quad (16)$$

The amplification coefficients, δ, are provided in Table B in the Appendix.

5 Conclusions

The study has shown that when dealing with ground motion caused by shallow and weak seismic sources like in the analysed case of mining induced seismicity, local conditions and their variability even over a relatively small area have significant influence on surface effects. In order to determine and predict ground effects due to such sources it is recommended to run dedicated dense monitoring networks and, when the acquired data allows, to construct local GMPE-s. The GMPE-s should in any case include site terms, either relative or absolute if known.

The amplitude of ground motion depends significantly on the source mechanism type. In the studied case it has turned out that the normal and odd faulting events induce in general stronger motion than the thrust faulting and non-DC events. If a ground motion database is enough big it is advisable to construct mechanism-specific GMPE-s. Obviously, one must have also a multisensor seismic system and a reliable software tool, together being capable to determine source mechanisms of even weak events.

The zone membership of seismic sources has proved to discriminate significantly the resultant ground motion amplitudes. It seems that the effect is rather related to mining conditions than to source locations. However, in order to explain the origin and mechanism of the observed relation between the ground effect and the zone membership further detailed studies are needed.

The studied database has been dominated by lower magnitude seismic events and consequently smaller epicentral distances. In these circumstances a weighted approach to GMPE identification may be more relevant. This will be a subject of a subsequent study.

6 Acknowledgements

This work was supported within statutory activities No 3841/E-41/S/2016 of the Ministry of Science and Higher Education of Poland.

7 References

[1] Ambraseys, N.N., and Douglas J. (2003): Near-field horizontal to vertical earthquake ground motion, *Soil Dynamic and Earthquake Engineering* **23**, 1-8.

[2] Ambraseys, N.N. and Simpson K.A. (1996) Prediction of vertical response spectra in Europe, *Earthquake Engineering And Structural Dynamics* **25**, 401-412.

[3] Ambraseys, N.N., Simpson, K.A., and Bommer, J.J. (1996) Prediction of horizontal response spectra in Europe, *Earthquake Engineering And Structural Dynamics* **25**, 371-400.

[4] Ambraseys, N.N, Douglas, J., Sarma, S.K. and Smit P.M. (2005) Equations for estimation of strong ground motions from shallow crustal earthquakes using data from Europe and middle east: horizontal peak ground acceleration and spectral acceleration, *Bulletin of Earthquake Engineering* **3**, 1-53.

[5] Bommer, J.J., Douglas, J. and Strasser, F.O. (2003) Style-of-faulting in ground motion prediction equations. *Bulletin of Earthquake Engineering* **1** (2), 171-203.

[6] Boore, D.M. and W.B. Joyner (1982) The empirical prediction of ground motion, *Bulletin of the Seismological Society of America* **72**, S43-S60.

[7] Cambell, K. W. (2003), Strong- Motion Attenuation Relations. **In**: *International Handbook of Earthquake Engineering Seismology*, volume 18B, (Lee, W. H. K., Kanamori, H., Jennings, P. C., Kisslinger, C. red.) Academic, Amsterdam, 1003-1012

[8] Douglas, J., (2003) Earthquake ground motion estimation using strong-motion record: a review of equations for estimation of peak ground acceleration and response spectral ordinates. *Earth-Science Reviews* **61**(1-2), 43-104.

[9] Frohlich, C. and Apperson, K.D. (1992): Earthquake focal mechanisms, moment tensors, and the consistency of seismic activity near plate boundaries. *Tectonics* **11** (2), 279–296.

[10] Gibowicz, S. J. (1990) Seismicity induced by mining. *Advances in Geophysics* **32**, 1-74.

[11] Gibowicz S.J. (1993) Keynote address: Seismic moment tensor and the mechanism of seismic events in mines, **In:** *Rockbursts and Seismicity in Mines '93* (ed. Young, R.P.) , A.A. Balkema, Rotterdam, pp. 149-155.

[12] Joyner, W.B., and D.M. Boore (1993): Methods for regression analysis of strong motion data, *Bulletin of the Seismological Society of America* **83 (**2), 469-487.

[13] Kawase, H. W. (2003), Site Effects on Strong Ground Motions. **In**: *International Handbook of Earthquake Engineering Seismology, volume 18B,* (Lee, W. H. K., Kanamori, H., Jennings, P. C., Kisslinger, C. red.) Academic, Amsterdam, 1013-1030.

[14] Kwiatek, G., Martínez-Garzón, P., and M. Bohnhoff (2016). HybridMT: A MATLAB/Shell Environment Package for Seismic Moment Tensor Inversion and Refinement. *Seismological Research Letters* **87** (4), DOI: 10.1785/0220150251..

[15] Lasocki S. (2002), Attenuation relation for horizontal component of peak ground acceleration below 10Hz frequency for Polkowice region, *Publications of the Institute of Geophysics, Polish Academy of Sciences*. **M-27** (352), 79-90 (in Polish, English abstract).

[16] Lasocki S. (2013) Site specific prediction equations for peak acceleration of ground motion due to earthquakes induced by underground mining in Legnica-Głogów Copper District in Poland, *Acta Geophysica* **61**, 1130-1155, doi: 10.2478/s11600-013-0139-8.

[17] Lasocki, S., Szybiński, M., Matuszak, J., Mirek, J. and A. Pielesz (2000), Prediction of surface vibrations caused by seismic events from mines: a critical revive, **In**: *Mat. Warsztaty Górnicze 2000 „Zagrożenia naturalne w górnictwie"* (Pilecka E. red), Wyd. IGSMiE PAN, 261-279. (in Polish, English abstract)

[18] Mutke, G. and J. Dworak (1992), Factors affecting the seismic effect of strong mining tremors on the surface structures in the Upper Silesia coal field, *Publications of the Institute of Geophysics, Polish Academy of Sciences* **M-16** (245), 115-129 (in Polish, English abstract)

[19] Olszewska D. (2006): Attenuation relation of acceleration response spectra of ground motion for the Polkowice region. *Publications of the Institute of Geophysics, Polish Academy of Sciences*, **M-29** (395).

[20] Olszewska D. (2008): Analysis of site effects and frequency spectrum of signals in order to improvement accuracy of attenuation relation of ground motion caused by mining induced seismic events in Legnica Głogow Copper district. *PhD thesis AGH University Science and Tec*hnology (in Polish, not published)

[21] Orlecka-Sikora, B. and Lasocki, S. (2002): Clustered structure of seismicity from the Legnica–Glogow copper district, *Publications of the Institute of Geophysics, Polish Academy of Science*, **M-24** (340), pp. 105–119 (in Polish with English abstract)

Table A – Amplification coefficients for mechanism-specific GMPE-s. Empty boxes occur when there were no records at the particular station from sources of the particular mechanism category.

Station Ordinal Number	Station ID Number	Logarithm of relative amplification, δ_k				
		Normal faulting	Thrust faulting	Odd faulting	CLVD	MIX
1	21	-0.204	-0.095	-0.033	-0.049	-0.167
2	22	0.025	0.135	0.082	0.040	-0.059
3	23	0.037	0.141	0.331	0.135	0.093
4	24	-0.047	-0.022	0.027	0.031	-0.122
5	25	-0.033	0.177	0.058	0.007	0.124
6	26	0.154	0.293	0.033	0.399	0.032
7	27	0.043	-0.062	0.136	0.031	-0.034
8	28	-0.354	-0.042	-0.181	-0.047	-0.136
9	29	0.034	0.041	0.204	0.035	0.007
10	30	0.315	0.155	0.149	0.190	-0.307
11	32	-0.025	0.112	0.301	0.080	-0.067
12	42	0.101	0.482	0.646	0.492	0.309
13	50	0.093	0.140	0.180	0.124	-0.006
14	51	0.021	0.198	0.245	0.133	0.155
15	55	0.173	0.081	-0.134	0.217	0.080
16	57	0.150	0.277	0.095	0.366	0.135
17	80	0.052	-0.029	0.004	-0.043	0.051
18	81	-0.027	-0.037	0.202	0.007	-0.124
19	82		-0.208		0.123	-0.031
20	83	-0.023	-0.084	0.018	-0.086	-0.200
21	84	-0.014	0.013	0.035	0.092	-0.049
22	20	0.0	0.0	0.0	0.0	0.0

Table B - Amplification coefficients for zone specific GMPE-s. Empty boxes occur when there were no records at the particular station from sources form the particular seismic zone.

Station Ordinal Number	Station ID Number	R2	R3	R6	R12	R13	R17	R22	R25	R26
1	21	-0.099	-0.129		-0.027	-0.185	-0.121	-0.314	-0.091	-0.139
2	22	0.041	0.293		-0.048	0.618	0.071		0.072	0.361
3	23		0.184		-0.106		0.148	-0.242	0.236	-0.176
4	24	-0.073	-0.026		0.017	0.014	-0.092	-0.260	-0.075	-0.289
5	25	-0.011	0.200	0.070	-0.436	0.988	0.119	-0.373		
6	26		0.038	0.251		0.829	0.369		0.149	0.344
7	27	-0.024	-0.080	-0.013	0.338	0.000	-0.065	-0.193	0.099	0.061
8	28		0.203	0.574				-0.282		-0.158
9	29	0.016	0.146	0.394	-0.185	0.560	0.158	-0.205	0.366	-0.116
10	30	0.195				0.327	0.109			-0.147
11	32	0.088	0.495	0.709	-0.171		0.446	-0.246	0.464	0.071
12	42	-0.027	0.539	0.885		1.085		0.147	0.857	0.675
13	50	0.093	0.242	0.527				-0.139		
14	51	0.161	0.260	1.024	-0.148	0.044	0.073	-0.220	0.766	
15	55	-0.121	0.240	0.392			0.105	-0.314		-0.041
16	57	-0.056	0.173	0.519			-0.117	-0.355	0.795	-0.185
17	80	0.127	0.060		0.095	-0.026	0.048	-0.144	0.024	-0.092
18	81	-0.109	-0.051	0.339	0.134		0.021	-0.141	-0.126	-0.278
19	82	-0.243	-0.003	0.414	-0.691		-0.445			-0.099
20	83	-0.176	-0.226	-0.141	-0.107	-0.001	-0.212	-0.522	-0.069	-0.163
21	84	-0.097	0.117	-0.023	-0.122	0.371	0.133	-0.287	0.040	-0.253
22	20	0.0	0.0	0.0	0.0	0.0	0.0	0.0	0.0	0.0